CANADIAN JOURNAL OF EXPLORATION GEOPHYSICS
VOL. 28, NO. 2 (DECEMBER 1992), P. 81-95

MODELLING OF GRAVITY ANOMALIES IN THREE DIMENSIONS USING NONLINEAR OPTIMIZATION

B.D. LONCAREVIC[1], M.E. BEST[2] AND W.A. KANTERS[1]

ABSTRACT

Our interest in determining the depth to sources led us to explore nonuniqueness of the interpretation of potential field data using nonlinear optimization. For a simple source body for which the horizontal block location and density contrast are defined and for measurements containing no noise, the procedure can fit a model as closely as desired. For a more complicated source body, for example a body with a gravity gradient, the shape of the calculated model is significantly different from the source body although the observed and calculated gravity anomalies match to any desired accuracy. The reliability of interpretation is further reduced when the observations are contaminated by noise and when the location of the model coordinates is displaced from the source coordinates. The excess mass of the source body is estimated for a number of optimization models with different densities. If the plan position of the model is fairly close to that of the source body then the density contrast can be estimated within reasonably narrow limits. To obtain the "best-fit", the model must be horizontally shifted when the source body has a vertical density gradient.

INTRODUCTION

The interpretation of gravity observations is an important geophysical method in exploration, in basin analysis interpretation, and in geodynamic modelling. It is cost effective and the results can be related to geological structures. The method has been in use for a long time (Nettleton, 1940; Dobrin, 1960) and in recent years has acquired a new power with the advent of digital computers and sophisticated computational algorithms (Talwani, 1965; Bhattacharyya, 1978; Nagy, 1988).

Two- and three-dimensional modelling of irregular bodies utilizes interactive graphic systems to compare observed and modelled gravity data. The standard approach to gravity modelling has been to calculate the forward gravitational anomaly of model bodies, changing body parameters until the observed and calculated gravity anomalies are in agreement (Haworth and Wells, 1980). This "forward modelling" can be time consuming. The selection of model parameters is subjective and arbitrary (in the absence of additional geological constraints), hence there is no assurance that an optimal model will be found.

The widespread application and use of computers has stimulated a development of automated procedures to derive a "best fitting model". (This is in quotations since solutions of potential field problems are not unique.) These procedures use nonlinear optimization criteria to deduce an optimal fit in a statistical (usually least squares) sense. Although they are sometimes called data inversions this is not strictly correct since the model equations have not been inverted. We will therefore describe our experiments using the term "nonlinear optimization" throughout this paper.

A number of two- and three-dimensional optimization techniques have been applied to gravity and magnetic data (Corbato, 1965; Johnson, 1969; Dyrelius and Vogel, 1972; McGrath and Hood, 1973; Oldenburg, 1974; Ku and Sharp, 1983; Silva and Hohmann, 1983; Chai and Hinze, 1988). Optimization schemes using multiple rectangular bodies for the modelling of gravity anomalies due to complex three-dimensional bodies with a vertical density gradient are treated less frequently in the literature (Cuer and Bayer, 1980). Our purpose in this paper is to investigate optimization of model bodies with nonlinear ridge regression techniques using the Levenberg-Marquardt Algorithm (LMA) (Levenberg, 1944; Marquardt, 1963). The software was made available to us by W. L. Anderson of the U.S. Geological Survey (Anderson, 1977) as an adaptation of the IBM Share Library Program No. 1428. There is nothing special about the choice of algorithm. LMA is robust and converges quickly under a wide range of conditions, although other algorithms may be better for different applications. Al-Chalabi (1971a) has used Rosenbrock's (1960) algorithm, while McGrath and Hood (1973) have used Powell's (1964, 1965) algorithm for three-dimensional optimization of magnetic data. Hjelt (1973) has published results of a comparison of three different methods of nonlinear optimization.

Manuscript received by the Editor August 19, 1992; revised manuscript received October 9, 1992.

[1]Atlantic Geoscience Centre, Geological Survey of Canada, Bedford Institute of Oceanography, P. O. Box 1006, Dartmouth, Nova Scotia B2Y 4A2

[2]Pacific Geoscience Centre, Geological Survey of Canada, P.O. Box 6000, Sidney, British Columbia V8L 4B2

We have benefitted from discussion with our colleagues at the Atlantic Geoscience Centre, Geological Survey of Canada. We thank particularly J. Verhoef and W. Roest for their comments on an earlier version of this manuscript.

The study was motivated by our interest in determining the depth to source of potential field anomalies. Therefore we allowed the depth parameters to be adjusted through optimization while keeping the position of the blocks fixed. Another approach would be to fix the depth parameters and allow the position of the sides of the blocks to be adjusted through optimization. We leave this second approach for a future study.

THEORY

We define the optimization problem in the following way. Given a set of observations (measurements), find the best estimate for the parameters of the physical model which describes them. The definition is general and not restricted to any particular model. The forward model therefore determines the optimization algorithm. With the above definition of the optimization problem, there is no restriction on the type of forward-modelling algorithm that can be used for 3-D gravity bodies. The main consideration should be the comparative efficiency and the ease of use.

Optimization methods look for an estimate of the physical parameters of the forward model which would give best-fit (in a least square sense) between the model response and the data. This is accomplished by locating the minimum of the objective function Φ. The objective function is given by the following expression:

$$\Phi = \frac{1}{N}\sum_{i=1}^{N} w_i\left[y_i - f\left(x_{1i}, \ldots, x_{mi}; b_1, \ldots, b_k\right)\right]^2, \qquad (1)$$

where N is the number of observations, m is the number of independent variables, and k the number of model parameters. Weights w_i, related to the accuracy of observations, can be assigned to each y_i. The model function (f) to be fitted to the observed data is a function of the independent variables x_l ($l = 1, \ldots, m$; $m > 1$) and the unknown model parameters b_j ($j = 1, \ldots, k$; $k > 1$).

A hypothetical example of the objective function for a 2-parameter model with parameter values b_1 and b_2 is shown in Figure 1. If the function of b parameters is linear, then the shape of the Φ surface is an ellipsoid of revolution with only one minimum. Generally, the parameters are nonlinear with the corresponding surface having more than one local minimum [for example, see figures 8 and 9 in Al-Chalabi (1971b)]. Several methods have been developed to find the minimum of the objective function. As already stated, we shall use the LMA algorithm (Levenberg, 1944; Marquardt, 1963; Tabat and Ito, 1973). This is a maximum neighbourhood method that performs an optimum interpolation between the Taylor series expansion method and the gradient (steepest descent) method. Without going into details, this algorithm expands the objective function into a Taylor series to handle the nonlinearity and combines it with a gradient method to find the minima. The method is robust and usually converges within a few iterations. After each iteration, the parameters are recalculated (iterated) by taking the computed gradients of the objective function with respect to the b's and algebraically adding them to the present values of b.

The objective function for the gravity problem is given in equation (1) with $y_i = g_i$ the observed gravity values (free-air or Bouguer) in milligals (mGals); $F = f$ the forward gravity model; x_i, y_i, z_i the coordinates of the ith gravity value; and b_j the model parameters. The model parameters are a combination of the body coordinates and the density of each block. The particular combination of model parameters is governed by the problem.

There are a number of algorithms for computing the gravity anomaly of 3-D bodies. We shall use a forward gravity model consisting of a number of rectangular blocks, each of constant density.

Our forward gravity model is based on rectangular blocks whose gravity values are given by (Banerjee and Gupta, 1977; Chai and Hinze, 1988):

$$f = G\rho \sum_{i,j,k=1}^{2} (-1)^{1+j+k} \tan^{-1}\left[A_i B_j / C_k R_{ijk}\right] \qquad (2)$$
$$-A_i \log\left(R_{ijk} + B_j\right) - B_j \log\left(R_{ijk} + A_i\right),$$

where $A_i = x_i - x$; $B_j = y_j - y$; $C_k = z_k - z$ with $i, j, k = 1$ the beginning block coordinates (b) and $i, j, k = 2$ the end coordinates (e) (see Figure 2). The function R_{ijk} is equal to $(A_i^2 + B_j^2 + C_k^2)^{1/2}$ and x, y, z are the coordinates of the observed gravity.

For a forward gravity model consisting of M such rectangular blocks, the beginning coordinates of block j are x_{bj}, y_{bj}, z_{bj}, and the end coordinates are x_{ej}, y_{ej}, z_{ej}. The density of block i is ρ_j. To obtain the total gravity effect from the m blocks, the contributions from each block are added together.

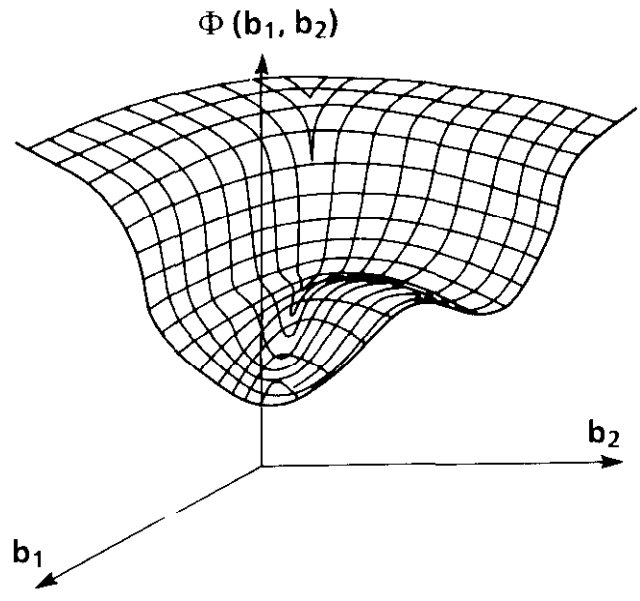

Fig. 1. An example of a two-dimensional surface of the objective function (Φ) for nonlinear parameters b.

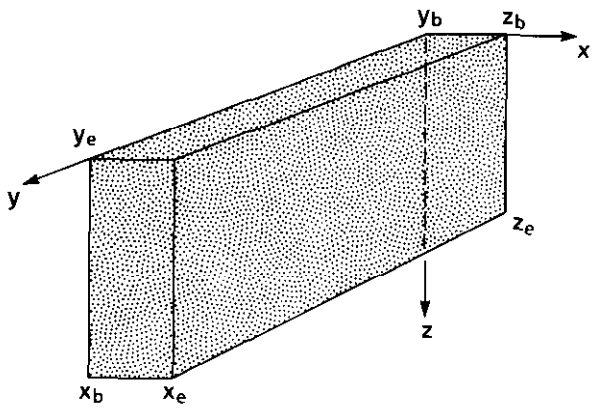

Fig. 2. Coordinate system and parameters defining a rectangular block. The beginning coordinates have the subscript *b* and the end coordinates have the subscript *e*.

$$F(x_i, y_i, z_i; b_1, \ldots, b_k) = \sum_{j=1}^{M} f(x_i, y_i, z_i; x_{bj}, x_{ej}, y_{bj}, y_{ej}, z_{bj}, z_{ej}, \rho_j). \quad (3)$$

In equations (2) and (3), note that the gravity function depends linearly on the density and nonlinearly on the coordinates (i.e., tan-1 and log functions).

A rectangular prism model is defined by two x, y coordinates of opposite corners and the depths of the top and bottom surfaces, a total of 6 parameters. With density as another adjustable parameter, there are $7*M$ unknowns for the M blocks. The choice of model parameters to fix or vary depends on the problem. If additional information is available from some independent measurement, then the range of solutions can be limited. For example, rock sample densities or density logs provide a constraint on the density while seismic sections provide a constraint on the structure.

Modelling Examples

In the remainder of this paper we describe a number of numerical experiments performed in order to gain insight and to understand better the practical applications of optimization procedures. We look first at a simple example consisting of three separate rectangular bodies. Next, we model a more complex source body consisting of three overlapping rectangular prisms. Finally, we look at a complex body composed of 16 prisms. The robustness of the method is tested by adding small amounts of random noise to the observed values of this model and by studying the effect of positioning of the model body (relative to the source) on the fit of the model. We look at the changes to the calculated excess mass as a function of density contrast and finally examine the effect of the vertical density gradient on the model results. In our terminology, "source bodies" are the initial mass configuration used to calculate the "observed" anomaly. "Model bodies" are the results of optimization. All the calculations are based on density contrasts.

Modelling of isolated sources

Two source bodies are used to investigate the limitations of the gravity optimization scheme using the LMA algorithm with the forward model as given in equations (2) and (3).

The source body (Figure 3a) consists of three rectangular blocks 2 km square with density contrasts and depths as given in Table 1.

The gravity values for this model are calculated on a uniform 1-km grid over the area AB′A′B in Figure 3a leading to the contour map in Figure 3b. These synthetic data are used as input (observed) data in the optimization program. There are 225 data points (N = 225) in the grid. The observation elevation is constant (z = 0), while the x, y values are computed every kilometre beginning at origin (0, 0) marked point A in Figure 3a. In this example, the two independent variables (m = 2) are the x_i and y_i values where the "observed" gravity values were "measured".

The total number of optimization parameters depends on the number of rectangular blocks and on the parameters allowed to vary. For example, if the corners (x, y coordinates) and the density contrasts of the three blocks are given (see Table 1) there are 6 parameters to fit (i.e., the top and bottom of each block). The optimization program requires initial estimates for the unknown parameters. Table 2 provides an estimate for these values as well as the values of the given parameters. The choice of initial values of the unknown parameters is arbitrary provided that they are reasonable in the context of the problem.

Figure 3c is the gravity contour map for the initial model in Table 2. These contours are very different from the "observed" contours in Figure 3b. The purpose of the optimization procedure is to adjust the model until the calculated anomaly due to the source body and the observed anomaly agree within a specified accuracy (as measured by their rms difference).

As mentioned earlier, the LMA algorithm uses a combination of Taylor series and gradient methods. In either case,

Table 1. Densities and depths for the source body in Figure 3a.

Block	Depth		Density Contrast
	Top (km)	Bottom (km)	(kg/m3)
1	.0	2.0	100.
2	.0	3.0	200.
3	.0	4.0	300.

Table 2. Values of the model parameters for optimization of the source body in Figure 3a.

Block Unknown	Known Parameters					Initial Estimates	
	Xb	*Xe*	*Yb* (km)	*Ye*	(kg/m^3)	*Zb* (km)	*Ze*
1	3.0	5.0	6.0	8.0	100.	0.5	4.0
2	8.0	11.0	4.0	6.0	200.	4.0	5.0
3	8.0	11.0	8.0	10.0	300.	1.0	2.0

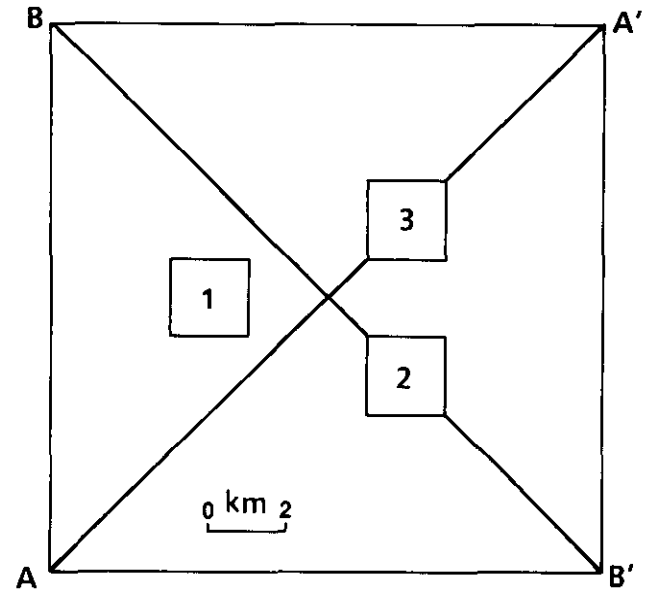

(a)

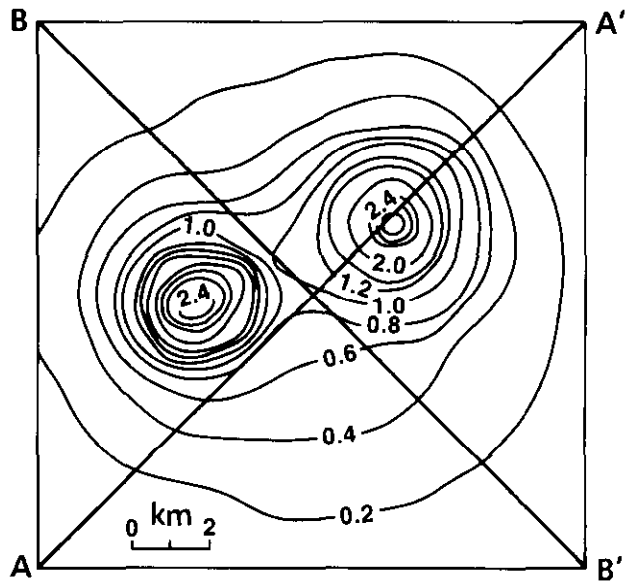

(c)

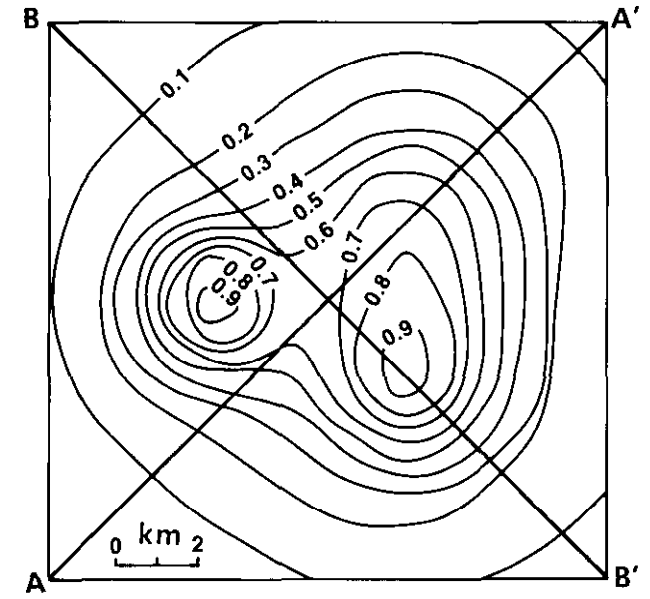

(b)

Fig. 3. **(a)** Plan view of source body number 1 consisting of three rectangular blocks. The origin is at *A*. Depths and densities are given in Table 1. **(b)** Calculated gravity contours for source body 1. The contour interval is 0.1 mGal. **(c)** Gravity contours for the initial parameters in Table 2. The contour interval is 0.2 mGal.

the derivatives of the objective function with respect to each of the b parameters must be computed. The Marquardt scheme provides an option to use either numerical or analytical derivatives. We compute numerical derivatives in the present version of the program. A one-sided derivative is generally all that is required. A more accurate two-sided derivative is automatically computed when additional accuracy is needed. Hence, the number of forward calculations for each iteration of the model parameters is at least $N + Nk = (k + 1)N$. For the above example, this means that at least 7 times 225 or 1575 forward computations per iteration are carried out.

After 6 iterations and 9450 forward computations, the optimization reached the accuracy specified. In this case, all final gravity values computed from the optimization are within 1 part in 10 000 of the observed values. (This convergence limit was chosen because in practice we may be measuring anomalies of the order of 100 mGal with a precision of 0.01 mGal, i.e., 1 part in 10 000). The depths for all three blocks were within a metre or so of the actual values. This is not surprising since only the depths were varied. All other parameters in the optimization were fixed at the *actual* values of the source body; this is a well-constrained problem. Rather than dwell on this simple case, we shall now investigate a more complicated body, resembling those found in nature.

Modelling of overlapping sources

In this example the source body has three rectangular blocks with the configuration shown in plan on the left in Figure 4 and in cross-section on top of Figure 5a. Depths and density contrasts of the three bodies are identical to those given in Table 1. Observed gravity values are calculated on the same 1-km grid as the first model. Note the observed gravity contours (Figure 5b) are symmetrical about the diagonal AA′.

The forward model for this example consists of a number of rectangular prisms of equal size. There are 16 blocks, each a cube with 1.5-km sides. Each block is numbered from 1 to 16 (Figure 4, right) and has initial top and bottom depths of 1.5 km and 3 km, respectively (Figure 5a, middle). The boundaries of the top (6 × 6-km area) source and model bodies coincide. The other two source bodies (with 4 × 4- and 2 × 2-km areas) deliberately do not coincide with model body sides. This was done in order to create a more complicated, and perhaps more realistic, example. The density contrast for this model is 100 kg/m^3.

The initial model gravity is symmetric while the observed gravity has a steep gradient over the area where the three bodies overlap (Fig. 5b). There are 225 observations with 32 parameters to fit (the top and bottom of each block); hence there are at least 33 times 225 or 7425 forward computations for each iteration. Where the density contrast of the source body increases (i.e., under blocks 6, 11 and 16) the optimization compensates by forcing the tops of these blocks closer to the surface while simultaneously increasing their depths. The differences between the final gravity values from the optimization and the observed values after 8 iterations or 59 400 forward computations are within 1 part in 10 000.

Figure 6 shows a perspective view of the optimized result for the 16-block model using a constant density contrast of 100 kg/m^3. The model has resolved the three layers, which is encouraging. Its shape is acceptable. The thickness is about 50 percent greater due to the smaller average density contrast of the model than that of the source body (100 vs. 142.8 kg/m^3). This density difference causes the corner block (16) to be particularly extended. The constraint imposed by the gravity gradient forces the two closest blocks (12 and 15) to be extended also. These three blocks overcompensate for the density difference. Block 11 is thinner than the source body so that the combined influence of these four blocks corresponds to the observed gravity. A similar overcompensation occurs with blocks 8 and 14 with block 6 undercompensating.

The optimization algorithm calculates the gradients of all adjustable parameters and then proceeds to make small adjustment to body parameters in turn, according to the "steepest-descent" principle (i.e., the parameter to be adjusted next is the one which will produce the biggest improvement in the fit of model to observations). We were concerned about the order and criteria used by the program during the optimization and therefore investigated how the individual block thicknesses varied from iteration to iteration.

Figure 7 shows the adjustment changes to the tops and bottoms of all the blocks model iteration. Note the symmetry of behaviour as expected from the symmetry of the source body (pairs 12-15, 11-14, etc. are identical). Note also the oscillating behaviour of the three blocks in the upper corner;

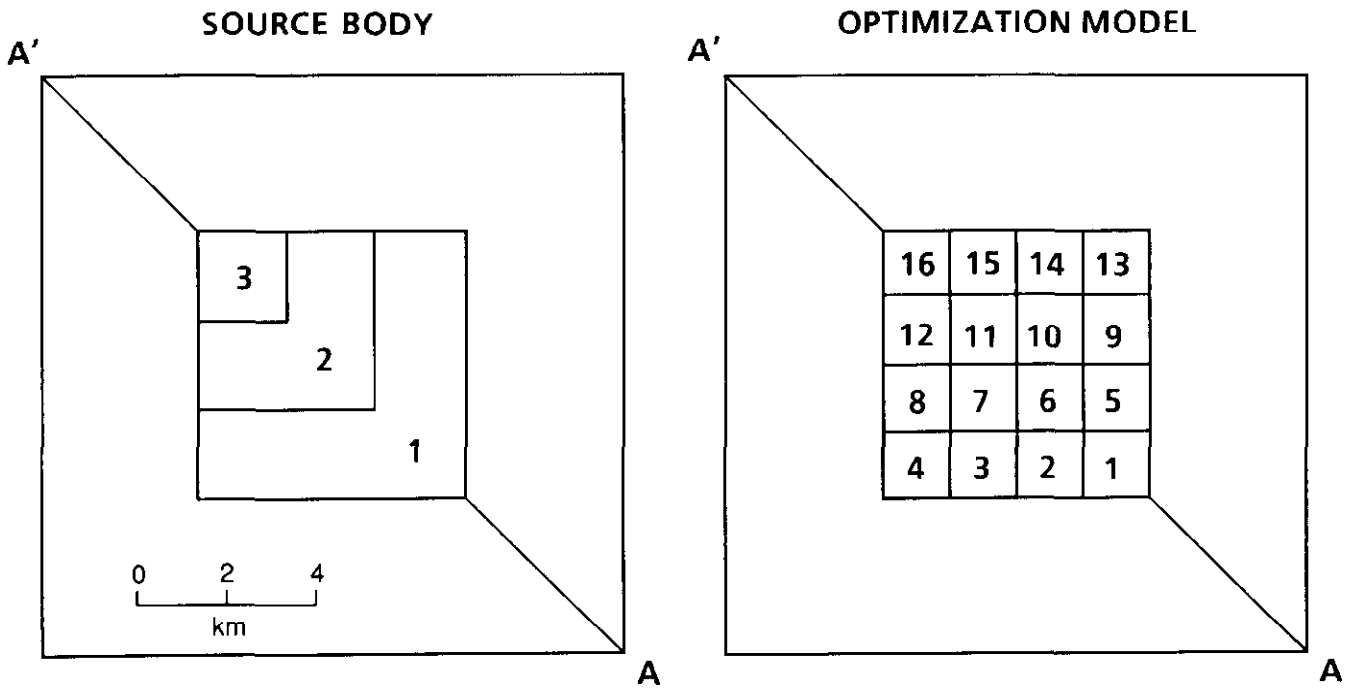

Fig. 4. Plan view of source body 2 consisting of three rectangular blocks. The origin is at *A* and the depths and densities are the same as those for source body given in Table 1. The optimization model consists of 16 blocks, each with an initial top and bottom depth of 1 and 3 km, respectively. The densities are discussed in the text.

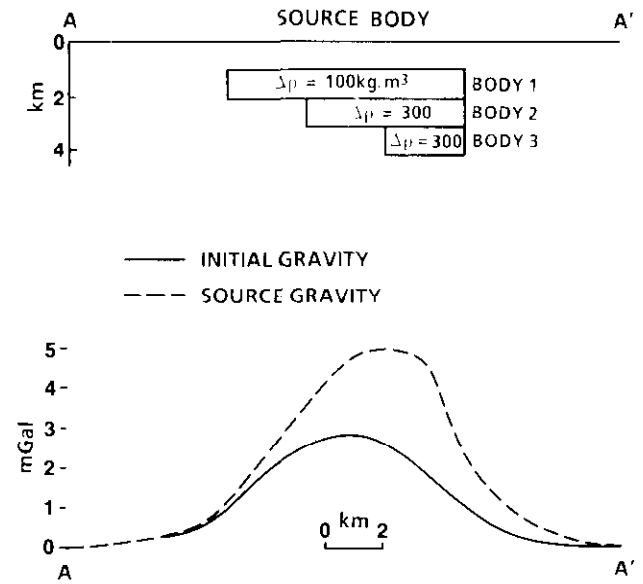

(a)

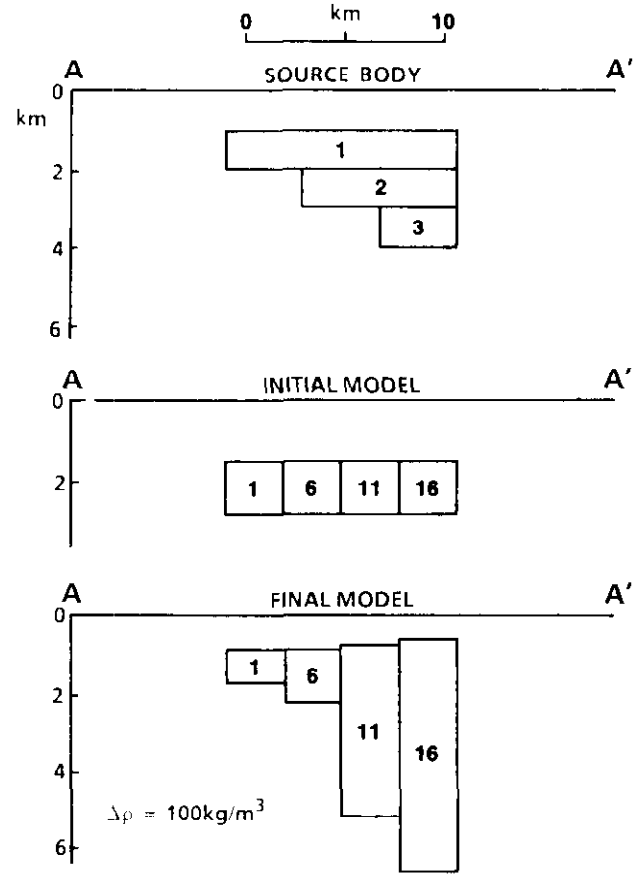

(b)

Fig. 5. **(a)** Source and initial model gravity profiles along *AA'* for the source body in Figure 4. The initial model has a constant density of 100 kg/m^3. **(b)** The top diagram is a cross-section along *AA'* for the source body in Figure 4. The middle diagram is a cross-section along *AA'* for the initial optimization parameters. The bottom diagram is a cross-section of the best-fit optimization model for a constant density of 100 kg/m^3.

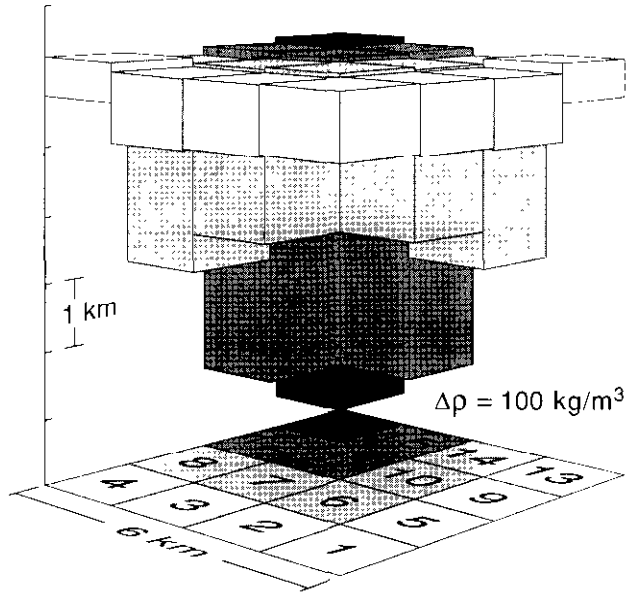

Fig. 6. Perspective view of the 16-block model of density contrast 100 kg/m^3 after 20 iterations. With "goodness-of-fit" factor (E) set equal to 0.05, the standard error (SE) is equal to 0.0276.

block 16 is out of phase with blocks 12 and 15. For the remainder of the blocks the first three steps are most critical. After that, the convergence towards the final model is smooth.

We were concerned about these different routes to convergence and conducted two experiments to test the robustness of the algorithm. In the first test we specified random order of the blocks in the initial model. In the second test we changed the initial model thickness. Both tests gave results similar to those discussed earlier, thus suggesting, at least in this case, that it is unimportant how the initial conditions, or order of model parameters, are specified.

Density changes in model blocks

The optimization model discussed so far assumed a constant density contrast of 100 kg/m^3. The model is quite different if we use a constant density contrast of 200 kg/m^3 (see Figure 8). The three-layer division is less obvious. The thickest block is not in the upper corner any more; it is now block 11. Continuity of gravity field forces down the surrounding blocks (7 and 10), resulting in a thin block 6 to compensate for mass excesses elsewhere.

We also tested the effect of a laterally variable density contrast by running the optimization with a density contrast of 200 kg/m^3 for all blocks except 1, 2, 3, 4, 5, 9 and 13 (see Figure 4) which had a value of 100 kg/m^3. The final and observed gravity values were again within 1 part in 10 000.

The best fit values of the top and bottom of each block, the number of iterations, and the initial and final values of the objective function and the standard error are listed in Table 3 for the three density models described above. The tops and bottoms of the blocks are at different levels for models with different assumed density contrasts, even though the observed and computed gravity values are almost

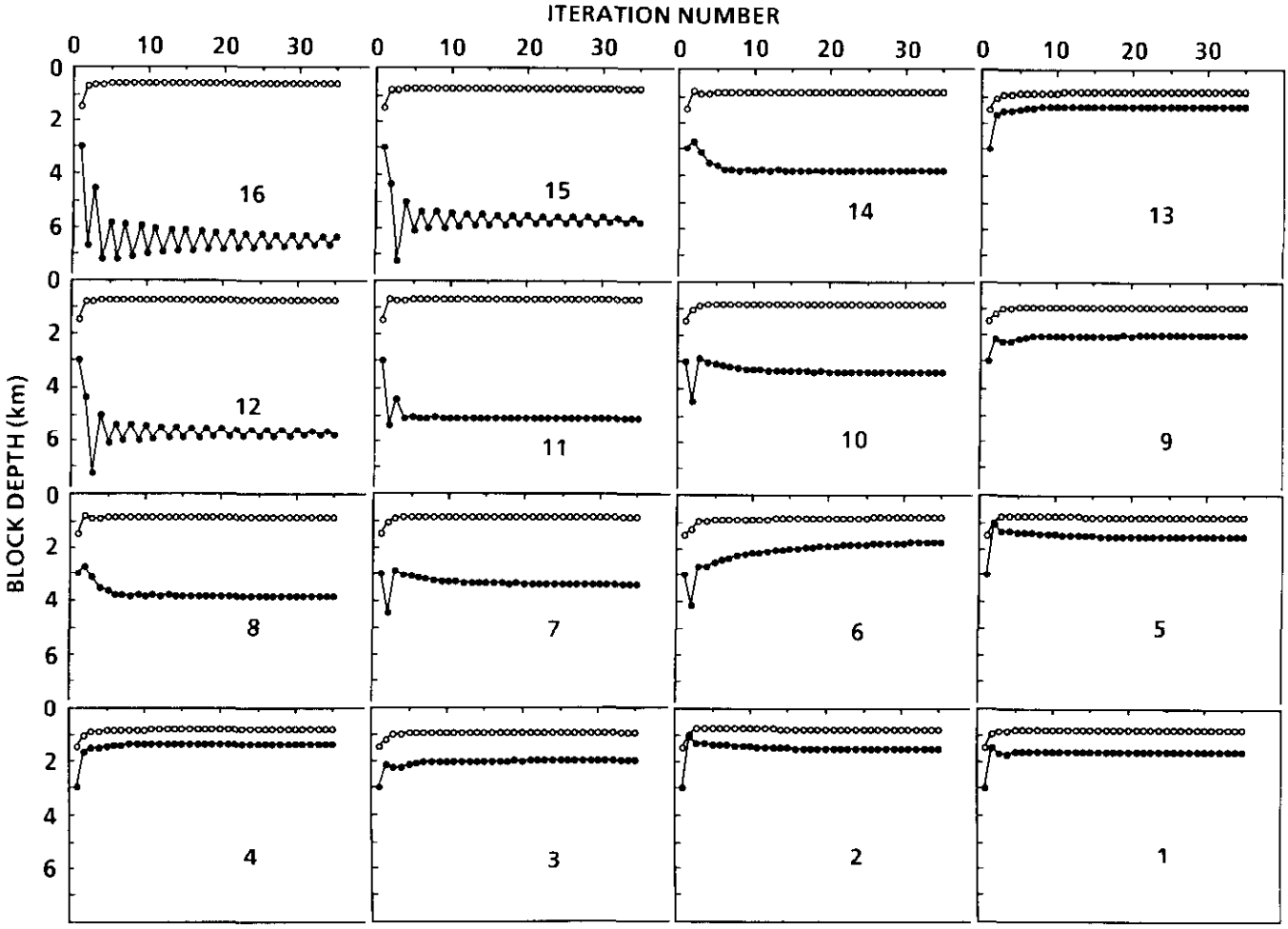

Fig. 7. The changes of the estimated depth for all 16 blocks at each step during iteration. Note the symmetry around the diagonal through blocks 1-16. Model blocks follow different paths toward the objective function minimum because of the asymmetry of the source body.

identical. All model bodies differ from the true depths of the source body. Of course, an optimization model with constant density in each block can never reproduce the source body which has a density contrast that varies with depth.

Two important points can be gleaned from this example. First, the final values of the objective function, standard error and number of iterations, are different for different models. From Table 3 we see that the two-density model has the smallest initial value of standard error and the objective function. The nonuniqueness of the problem is quite clear from the results given in Table 3, although both constant and variable density contrasts give good fits to the observed data. If the number of blocks or the areal coverage of the blocks is changed, this too will affect the solution space. This shows the importance of constraining the parameters independently using geological and geophysical information.

The experiments described so far show that LMA will produce a numerical agreement between the observed and model results – which is not surprising. The simple simulation experiments do not throw any light on the limitations of the nonlinear optimization procedures. To gain that insight, we carried out additional numerical experiments.

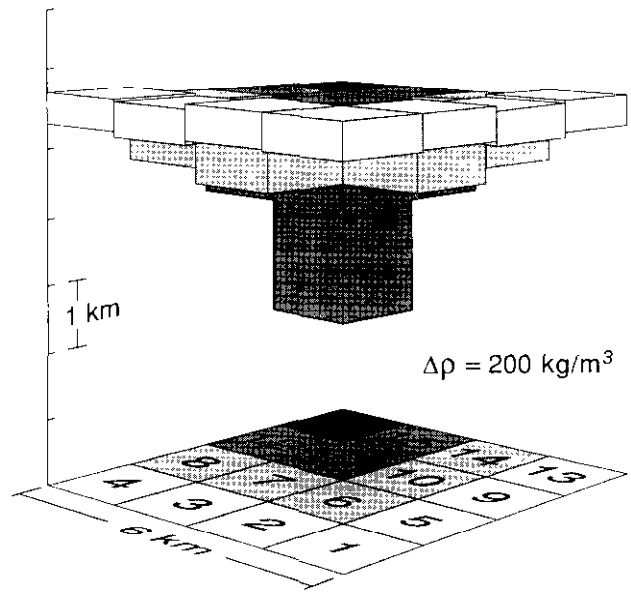

Fig. 8. Perspective view of the 16-block model of density contrast 200 kg/m^3 after 6 iterations. E = 0.05, SE = 0.0389 (compare with Fig. 6).

Addition of random noise

In practical surveys the observations are contaminated by noise; the position of the model body with respect to the observed anomaly is not known, and the density contrast (and its variation with depth) causing the anomaly is unknown and must be assumed. We investigated these three effects (noise, position and density) on the optimization models with surprising results.

A three-layer source and 16-block model body (with density contrast of 100 kg/km^3) were tested by adding random Gaussian noise to every observed data point. Two hundred and forty-six optimization runs were performed with a range of randomly selected noise values between 0.01 and 0.28 mGal (+/- 0.14 mGal). The result is shown in Figure 9. The x-axis shows the range of random noise applied for different runs while the y-axis shows the standard deviation of the 16 blocks of the "noisy model" relative to the "noise-free" model.

As expected, adding noise to observations produced optimization models quite different from the noise-free model. We did not expect to discover that the effect of noise could be so significant. The total range of the observed anomaly for our case is 0 - 5 mGal. Adding only a few tenths of milligals of random noise significantly distorts the model. Identical amounts of noise produce different models which can be very different (see the dispersion in Figure 9). Significantly, once noise is introduced there is a lower limit to the standard deviation, i.e., there appears to be no particular distribution of noise that would cancel itself and produce a model with the same standard deviation as the noise-free model.

Table 3. Final estimates for the top and bottom of each of the 16 blocks (in metres) for three density models. SE is the standard error which is the square root of Φ/number of degrees of freedom where the number of degrees of freedom is (N - k). PHI is the value of the objective function. It is a least-squares measure of the goodness-of-fit.

Density Block Number	100 Top / Bottom	100 & 200 Top / Bottom	200 Top / Bottom
1	897 / 1770	993 / 2025	1194 / 1693
2	914 / 1771	992 / 1992	1194 / 1661
3	913 / 1827	1059 / 2095	1253 / 1234
4	801 / 1326	1041 / 1968	1212 / 1653
5	914 / 1771	992 / 1992	1194 / 1661
6	889 / 2268	1129 / 1640	1203 / 1764
7	872 / 3221	1350 / 2381	1363 / 2524
8	882 / 3831	1331 / 2314	1333 / 2290
9	913 / 1827	1059 / 2095	1253 / 1734
10	872 / 3221	1350 / 2381	1363 / 2524
11	778 / 5154	1365 / 4571	1380 / 4625
12	751 / 5845	1332 / 2906	1336 / 2908
13	801 / 1326	1041 / 1968	1212 / 1653
14	882 / 3831	1331 / 2314	1333 / 2290
15	751 / 5845	1332 / 2906	1336 / 2908
16	651 / 6331	1338 / 4810	1338 / 4749
SE (Initial)	0.7041	0.1727	0.6114
SE (Final)	0.0277	0.0119	0.0039
PHI (Initial)	95.69	5.75	72.14
PHI (Final)	0.1481	0.0274	0.0029
Iterations	9	5	6

Position of model body relative to the source

Our next experiment consisted of testing the sensitivity of the LMA procedure to the placement of the model body relative to the source body. For this experiment we displaced the model body along the diagonal A-A′ in steps of 141 m (i.e., 100 m × $2^{1/2}$).

For an initial trial we simplified the model body and replaced the 16 blocks with a single block to see if a minimum in the Standard Error can be detected. As can be seen in Figure 10, the minimum is unambiguous for a one-block model. It occurs when the model is displaced 0.7 - 0.8 km relative to the source body. The result can be explained with a qualitative argument. In this case, the model has constant density and only two adjustable parameters, the top and the bottom (i.e., the thickness) of the body. The mass of the source body is concentrated in one corner and the model has to be shifted in that direction to compensate for this asymmetry.

The second (lower) graph in Figure 10 shows the results when the 16-block model body is translated a similar distance. Since there are more degrees of freedom to adjust (16 tops and 16 bottoms of the blocks) the minimum is broader and is located closer to the zero diagonal displacement. Note that there are several other local minima on this curve.

It is possible to modify the LMA program to let the optimization shift the horizontal position of the model body. (The common corners of adjacent bodies would have to move together so that there are no gaps and no overlaps between blocks.) In that case, it is possible for optimization to be "trapped" by one of the local minima and to converge to an incorrect position. More importantly, the number of

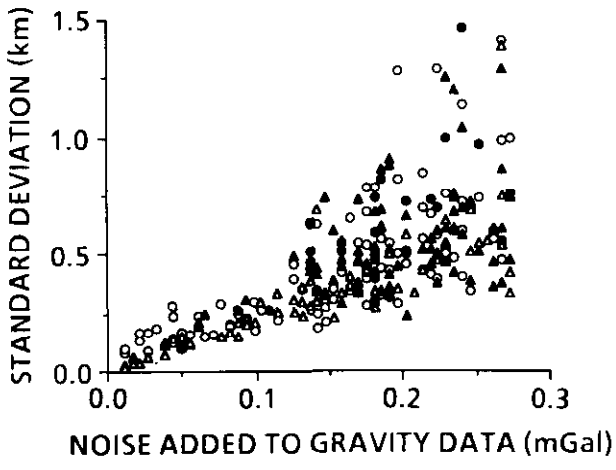

Fig. 9. The effect of random noise in "observations" (derived from source body) on the optimization. The standard deviation of the "noisy model" (y-axis) is relative to the "noise-free" model. Two different cutoff accuracies were used (circles — 0.05; triangles — 0.01). Open symbols indicate models which converged before the 36 iteration limit was reached.

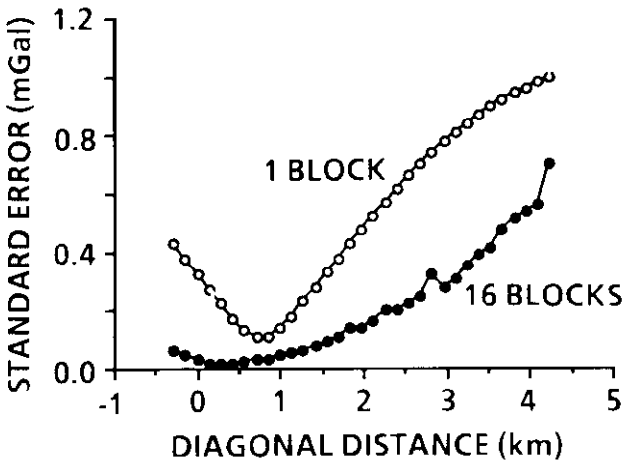

Fig. 10. Standard error (as a measure of goodness-of-fit) plotted against the displacement of model body relative to the source body. Model consisting of a single block gives a minimum standard error when displaced 0.7-0.8 km along the diagonal. Model consisting of 16 blocks has more adjustable parameters and consequently the broad minimum is located closer to the zero-displacement position.

adjustable parameters would increase greatly and the procedure would be dangerously unconstrained.

This is an important point and to investigate it further we have plotted the tops and bottoms of all 16 blocks for the model body as they are translated along the diagonal (Figure 11). Note that each block has sides of 1.5 km and therefore the diagonal distance of 2.115 km represents a "one-block step".

Figure 11 shows the response of all block tops and bottoms as a function of lateral translation. For distances less than one-block step, the behaviour of all blocks is predictable and understandable. The thickness of the blocks near the corner of mass concentration (i.e., 8, 12, 14, 15 and 16) decreases while the thickness of the blocks in the opposite corner increases (1, 2, 3, 5, 9). For the blocks in the middle the response is more complicated. Block 6 becomes negligibly thin and then rather suddenly drops to a depth of 9 km (the limit set for these runs). Blocks 7, 10 and 11 show similar wild oscillations. At greater diagonal displacements, blocks 4, 8, 12, 13, 14, 15 and 16 "flip" (tops become bottoms) indicating that negative density contrasts are needed to achieve the optimization convergence.

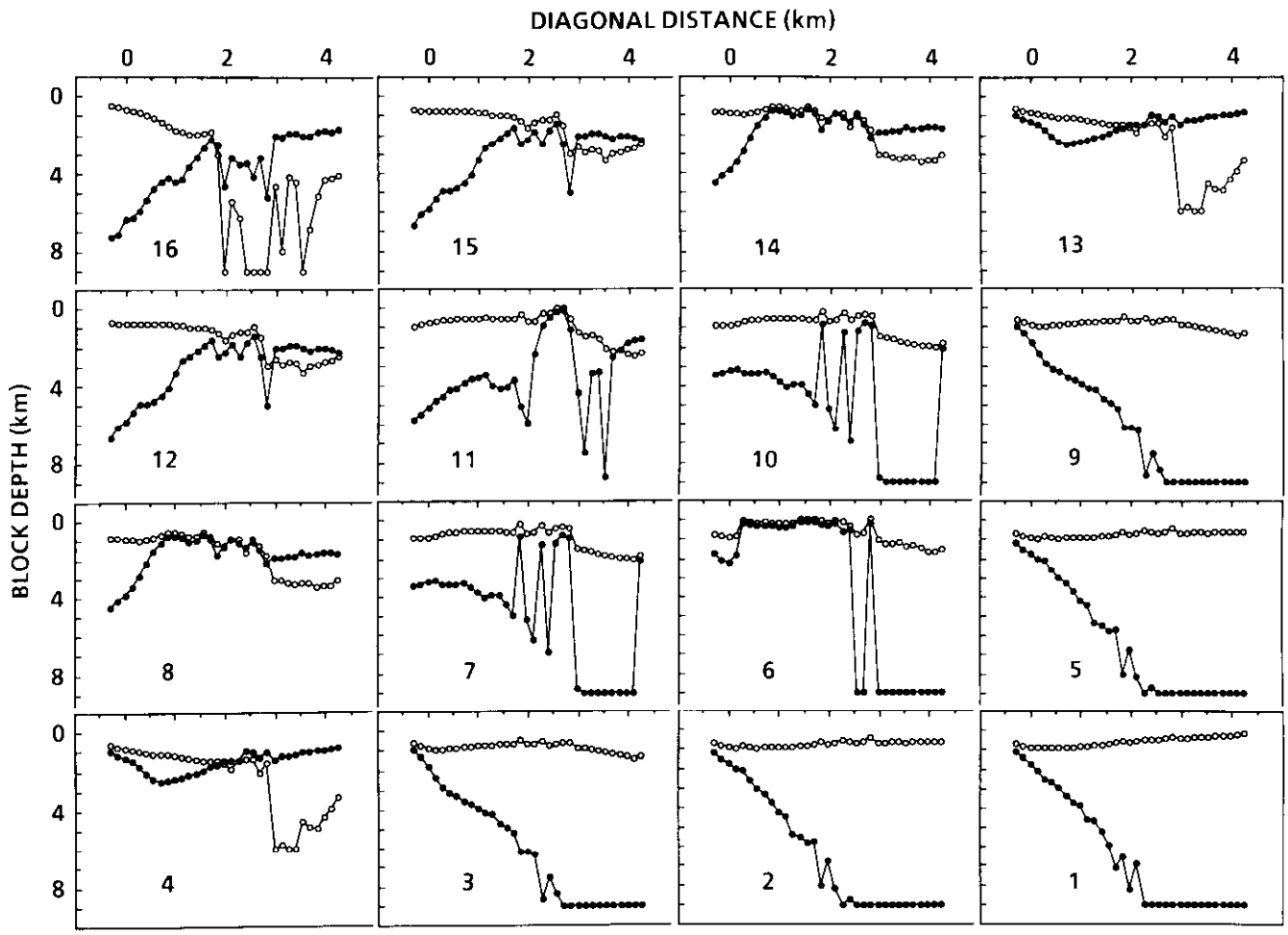

Fig. 11. The changes of the depth of the tops and bottoms of all blocks as a function of translation distance. For distances less than one-block step the behaviour of all blocks is predictable and understandable.

The effect of density and the estimation of the excess mass

Previous discussion has shown that unconstrained optimization cannot model the shape of the source body reliably when the density contrast (and gradient) and the horizontal position (and volume) are not known. From theory we know that the integration of the gravitational anomaly yields the total excess mass (see, for example, Grant and West, 1965; Telford et al., 1976). We conducted a number of numerical experiments to see under what conditions the optimization calculates the correct mass excess and to see how closely the density contrast of the source body can be estimated.

We started with a simplified source body consisting of a single block of $6 \times 6 \times 1.556$ km and density contrast of 143 kg/m^3. The excess mass of this body is 8.010188×10^{12} kg which is close to the excess mass of the three-layer source body discussed earlier ($6 \text{ km} \times 6 \text{ km} \times 1 \text{ km} \times 100 \text{ kg/km}^3 + 4 \times 4 \times 1 \times 200 + 2 \times 2 \times 1 \times 300 = 8.0 \times 10^{12}$ kg). The forward calculation of the gravity anomaly due to this body calculated on a 30×30-km grid with 2-km grid cell size constituted our "observations" to be modelled by 16 rectangular blocks with 1.5-km sides and with the depth of tops and bottoms as adjustable parameters.

Fifty optimization runs were performed with different starting density contrast, increasing in steps of 10 kg/m^3 between 50 and 550 kg/m^3. The results are shown in Figure 12. There is a minimum in the curve at a density contrast of 140 kg/m^3, the nearest point to the source body of density contrast 143 kg/m^3. The minimum mass is 8.001×10^{12} which is close to the exact value (given above). As the density contrast is increased, the excess mass is slightly overestimated. As the density contrast is decreased below the true value the overestimate of the excess mass increases rapidly.

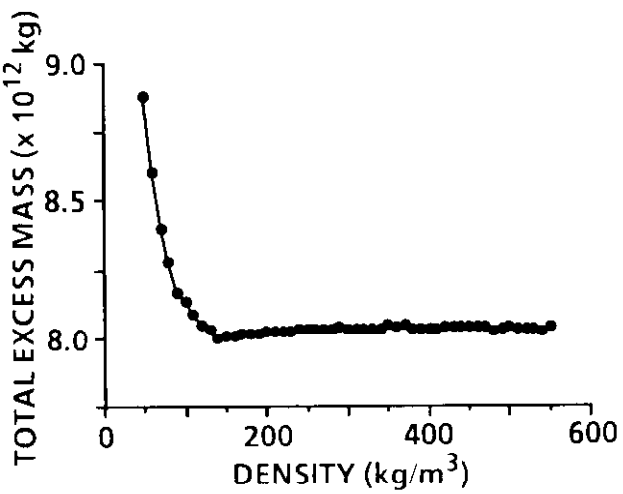

Fig. 12. The total excess mass of the model body for different assumed densities. There is a minimum at a density contrast of 140 kg/m^3, the nearest point to the average density contrast of the source body (143 kg/m^3). The excess mass value is also close to that of the source body.

To understand better the optimization process as a function of changing density contrast, we plotted the tops and bottoms of the blocks for all runs (see Figure 13). Near the correct density contrast, all the blocks are at the correct depth (tops at 1.0 and bottoms at 2.556 km). For smaller density contrasts all the blocks are thicker in order for the product of volume times density contrast to remain constant, i.e., equal to the total excess mass. For larger density contrasts, the outer blocks (represented by 16, 15 and 12 in Figure 13) are thinner than the source body but the inner blocks (e.g., 11) are thicker. The change occurs just before the correct density contrast is reached when the solutions suddenly jump to a different local minimum.

The thickness of the model blocks at low densities is greater than the source body, thus overestimating the excess mass (see Figure 12). The reason for this is not clear, but we suspect that it may be due to the limited extent of observations, truncated at +/- 15 km from the centre of the source body. Further evidence for this will be discussed later.

At very large density contrasts, the successive solutions become unstable, oscillating between different local minima. It is clear from qualitative considerations that as the density contrast increases, thinner and thinner blocks will be required to produce the observed anomaly. If we keep increasing the density contrast, eventually some blocks will flip, i.e., the tops will become bottoms.

Vertical displacement of the model

In the preceding example, the starting depths for tops and bottoms of all blocks were set at 1 and 3 km for each run. The model thus encompassed the source body. In the next experiment we set the initial tops and bottoms at 3 and 5 km. The result of excess mass calculations is shown in Figure 14. In this case, the optimization path is quite different with different initial conditions: there is no clear minimum at the right density contrast and total mass, though the points approach the correct value asymptotically near the correct density contrast.

The surprising feature of this experiment is the second level of stable excess mass estimation around 7.7×10^{12} kg between the density contrasts of 250 and 460 kg/m^3. This is followed by a sudden large jump to an even lower estimate.

The cause of this strange and unexpected behaviour is found in the plots of top and bottom depths of different blocks shown in Figure 15. Up to the density contrast of 250 kg/m^3 the tops and bottoms follow a predictable curve converging to the right configuration at the correct density contrast. At a density contrast of 250 kg/m^3 the system "breaks down" with corner blocks (16) flipping to a negative density contrast, i.e., the depth of top becomes greater than the bottom. This situation continues until the density contrast is 460 kg/m^3 when two other outer blocks flip (15 and 12) and the corner block (16) almost disappears (i.e., tops and bottoms almost coincide). It is therefore left to the central core blocks (11) to produce all of the observed anomaly, so these blocks become very thick.

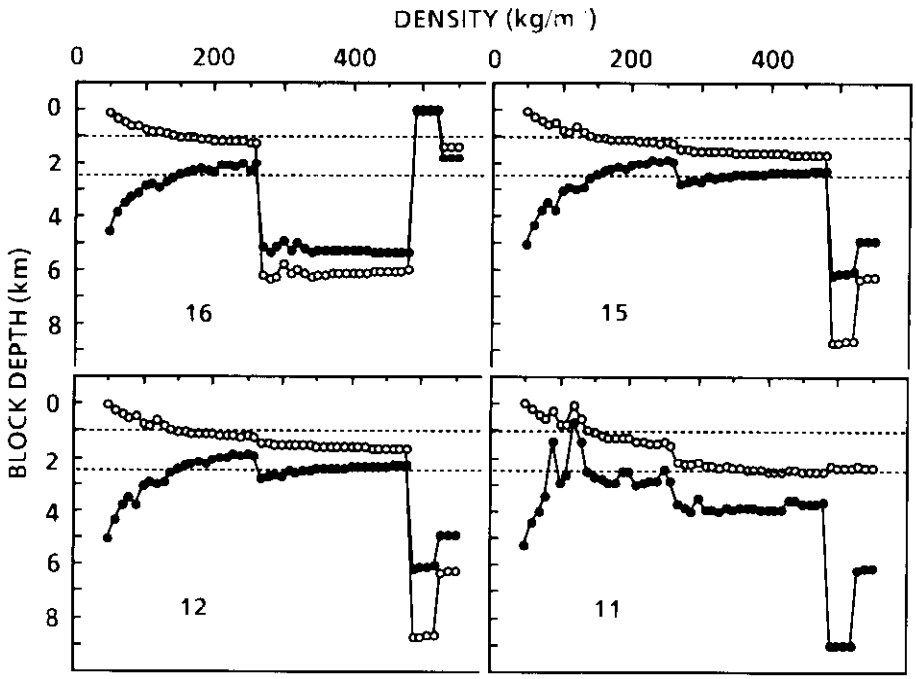

Fig. 15. Changes in the depths of tops and bottoms of blocks as a function of assumed density for initial depths of blocks set to 3 and 5 km (dashed lines).

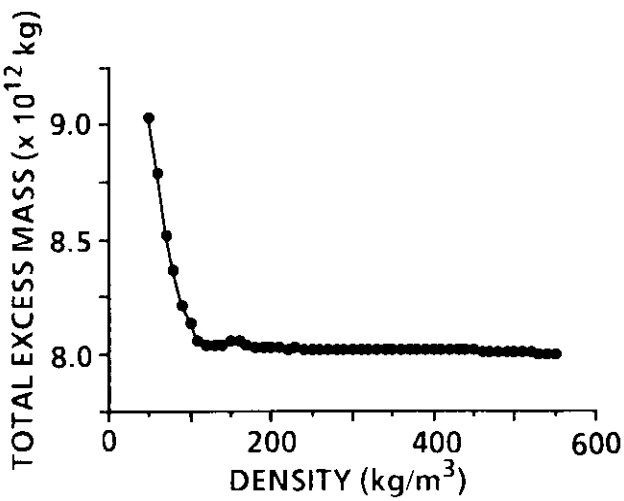

Fig. 16. The excess mass versus the assumed density contrast when the model body is displaced by 200 m (10% of a block side), which corresponds to the minimum in Figure 10.

The convergence towards a minimum excess mass is more rapid and the identified density contrast at minimum excess mass is lower in the case of the gradient decreasing with depth. In this case, as well as in the case of positive gravity gradient, the excess mass increases with increasing density contrast. This we attribute to the truncation of the observations. When the optimization runs were repeated with the observation points on a 30 × 30-km grid (2-km cell size) the excess mass increase beyond the density contrast of 200 kg/m^3 was much diminished. These experiments suggest that even in the case of a source with a vertical gravity gradient, the total excess mass can be estimated with some confidence provided the model body is located properly with respect to the source. The estimate of density contrast is much less reliable and seems to be on the high side in the case of the positive gravity gradient. The best we can do is to estimate the range of density contrast within about 50 kg/m^3.

Discussion and Conclusions

We have tried to demonstrate the limitations in using "black box" approach to nonlinear optimization by running numerous numerical experiments. The inversion of potential field data is a nonunique process and should not be carried out without the inclusion of other geophysical and geological constraints. In spite of these limitations, the nonlinear optimization should not be abandoned as an interpretation tool provided the interpretation is based on a sensitivity and robustness analysis along the lines discussed in this paper.

Our experiments lead us to make a number of observations:

(i) We believe that the most sensitive parameter is the horizontal location of the model body relative to the (usually unknown) position of the source body. It is important to shift the position of the model body around the expected position of the source body and to plot the tops and bottoms of all blocks in the model body. This process should lead to increased confidence that the optimization produces geologically and physically reasonable bodies.

(ii) The best-fit horizontal position of the model body depends (among other things) on the vertical density gradient in the source body. When a body with a nonzero vertical gradient is modelled with blocks of

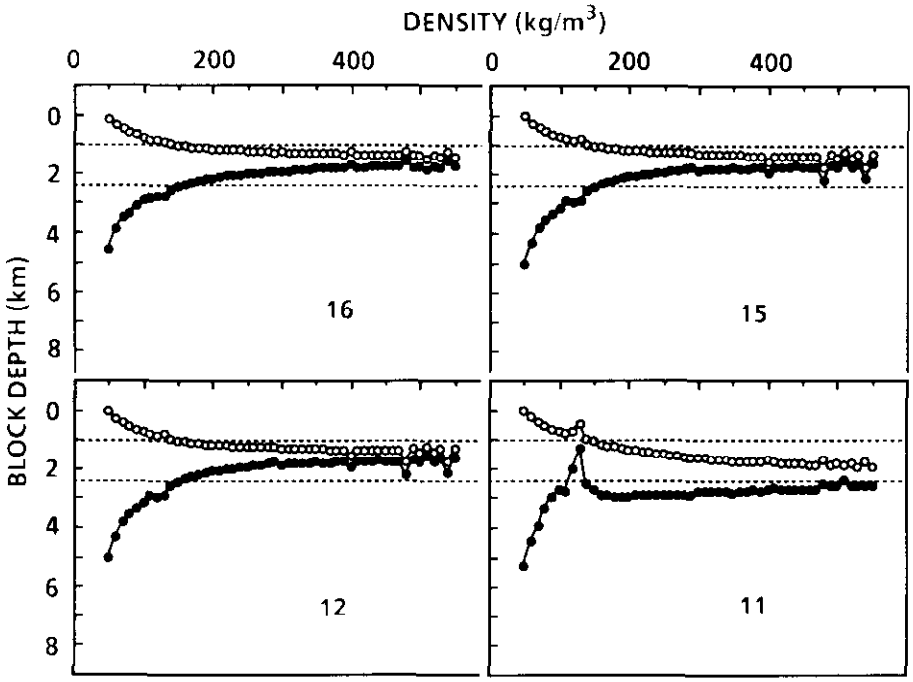

Fig. 13. Changes in the depths of tops and bottoms of blocks as a function of assumed density. Note that since the source body is axially symmetric around the diagonal, only four blocks in any one quadrant need be plotted.

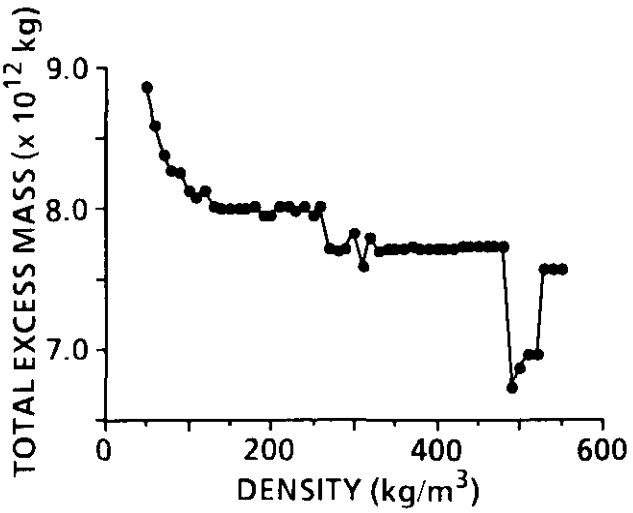

Fig. 14. The excess mass versus the assumed density for the initial tops and bottoms of model blocks set to 3 and 5 km.

It should be stressed that in all of the above examples, the calculated anomaly of the optimization models fitted the observations within the specified accuracy. Even in the case of such simple examples, the models resemble the source body only under very limited conditions. A single optimization, using only one set of initial parameters (for density and depths of tops and bottoms) is unreliable. To establish any confidence in the modelling process a series of experiments must be carried out to gain an appreciation of the behaviour of the optimization procedure as a function of the parameters.

Horizontal displacement of the model

In the next set of experiments, we displaced the location of the source and model bodies along the diagonal by 200 × 200 m, corresponding to 0.1 of a block size. The excess mass vs. density relationship is shown in Figure 16 and the tops and bottoms of blocks as a function of density contrast in Figure 17. There is evidence, in the jaggedness of the graph, of solutions converging towards different local minima. The minimum of the excess mass vs. density curve is identified at 250 kg/m^3, much larger than the correct value of 143 kg/m^3.

The displacement of 200 x 200 m of a body of dimensions 6 × 6 km is not very large, yet the results are so different from those discussed in Figures 12 and 13. This emphasizes once again the importance of the position of the model body with respect to the source body. In practice, of course, the position of the source body is not known. It is the purpose of the interpretation to find it. As we see from the above example in the interpretation of the field results, no conclusions should be drawn from a limited number of optimization runs without a systematic search of the parameter space.

Reversal of density gradient

For the final set of experiments, we used again the three-layer source body (described before in Table 1) but with density contrast decreasing with depth by assigning densities of 175, 100 and 25 kg/m^3. The densities were chosen in such a way as to obtain the same excess mass of 8.00×10^{12} kg and the same average density contrast of 143 kg/m^3 as we had before. These models were calculated with the observations on a 15 × 15-km grid with 1 × 1-km grid cells. The results are shown in Figure 18.

constant density contrast, then the calculated best-fit position of the model will be shifted horizontally relative to the source body.

(iii) One or more of the following may cause the solution to be unstable, i.e., small displacements of the model body may cause large changes in the model: (a) the trial location is a long way away from the correct position; (b) the number of parameters (blocks) and/or their distribution throughout the model is incorrect; and (c) the density choices are incorrect.

(iv) The amount of random noise in the observations may be a limiting factor in using an automated optimization procedure. On the basis of our experiments, we feel that noise greater than 5 - 10 percent of the peak value of observed anomaly may lead to geologically unrealistic or incorrect models. We have not investigated correlated noise, for example, in marine surveys when the readings along a track line are systematically high or low with respect to the adjacent lines.

(v) It is easy to obtain a good agreement between the observations and calculated values using automated procedures. Unwarranted confidence in the interpretation may occur if only agreements between profiles or contoured values are considered. It is important to study the shape of the model body and critically examine its geological plausibility.

The LMA converged towards a minimum in all of our tests, but the shape (i.e., tops and bottoms) of the fitted blocks differed from the observed body on every run. We conclude that without some additional constraints from geology or other geophysical observations, we have no confidence that the LMA models will approach the shape of the true body. Uncritical use of optimization procedures is more than likely to produce misleading geological interpretations.

Our overall conclusion is that "black box" optimization methods should be used with the greatest care. The data must be free of noise as far as possible. A systematic search of the parameter space should be undertaken to assess the sensitivity of different parameters. Such a search is slow on today's batch-job computers and requires patience and disproportionate resources. This situation is bound to change since the computing technology is evolving at a rapid rate. We envisage in the not too distant future a super-fast graphics work station where the number of parallel optimizations can be

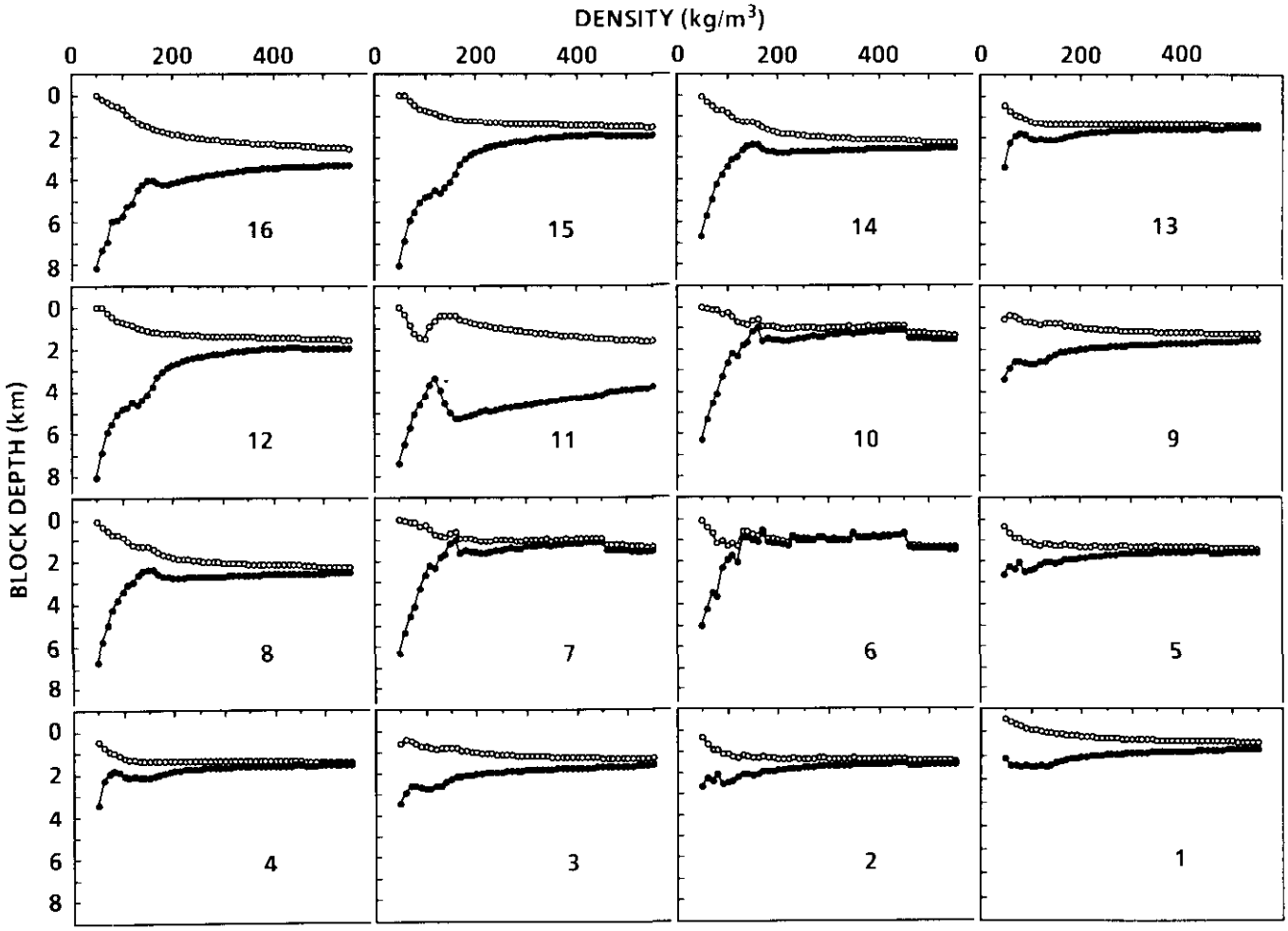

Fig. 17. Changes in the depths of tops and bottoms of blocks as a function of assumed density contrast for the model body displaced by 200 m.

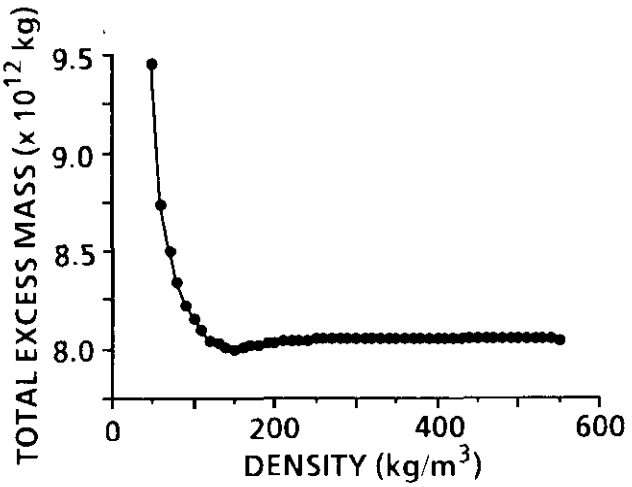

Fig. 18. The excess mass versus the assumed density contrast relationship when the contrast of the source body decreases with depth. The convergence towards a minimum excess mass is more rapid and the identified density contrast at minimum excess mass is lower, compared with the case when contrast increases (compare with Fig. 12).

performed while the parameters are changed interactively using a mouse or some other pointing device. Such an exploratory approach could be used to constrain the parameter space and thus limit the number of acceptable models. In spite of these improvements, the confidence limits when there is a vertical gradient decreasing with depth may be too wide to be of practical use without other independent constraints from geology or other geophysical measurements.

If the approach described in this paper is to be pursued, the software should be optimized for speed. For example, a look-up table for log and $\tan^{-1}$ could be calculated during the initialization of the program. Instead of calculating arc tangents and logarithms for each corner, interpolation in the look-up table should increase the processing speed by a factor of 100 or more for single runs. There are other improvements in algorithm speed that should result in several orders of magnitude increase in overall speed of data processing.

The present investigation could be broadened by studying the joint optimization of magnetic and gravity anomalies (Goodacre, 1973). In practice this introduces new sets of problems because of the unknown remanent magnetization and greater variability of susceptibility throughout the source body. If it could be established, on the basis of known geology and/or drill cores and logs, that the sources of magnetic and gravity anomalies are identical, then the joint optimization may prove to be a sufficiently constrained procedure to be of significant practical value in geophysical exploration.

The study reported here could be extended in several directions. The use of horizontal positions of the blocks as adjustable parameters in place of the depth of block tops and bottoms has already been mentioned. If all the blocks move rigidly relative to each other but have different tops, bottoms and density contrasts, the number of adjustable parameters (degrees of freedom) would be significantly reduced. As shown, the vertical gradient of density would shift the position of the models unless the model blocks were divided into several layers of density. Extending the work further by introducing the thickness of each layer as another adjustable parameter would require substantial modifications to the software to force the adjacent surfaces to move together; otherwise overlaps of blocks or gaps between them could easily happen.

We have used multiple blocks of equal plan area. It may be instructive to search for an optimum distribution of areas of blocks by allowing larger blocks in the centre if the source body is expected to be symmetrical. Sides of individual blocks could be set as adjustable parameters but again software must force joint adjustments to adjacent sides. (We have deliberately chosen an asymmetrical source body for our study to investigate a more difficult case.)

The relation between the given information (number of data points) and the number of degrees of freedom (adjustable parameters in the model) has not been investigated. Parker (1974, 1977) has shown that only three gravity points are necessary and sufficient to derive all the information about the "ideal bodies". Our approach attempts to go beyond his "ideal bodies", as one must when interpreting exploration data. We have used 225 regularly spaced data points but that number does not seem sufficient for the effects of noise to cancel. It would be a useful guide for an exploration manager to know the minimum number of field data required to define the source body within the limitations of the procedure discussed.

Finally, the nonlinear optimization techniques used by us are less sophisticated compared to, for example, Bayesian inversion techniques that treat the data and a priori information in a probabilistic manner (Jackson, 1979; Duijndam, 1988). We encourage others interested in this topic to carry out numerical experiments similar to the ones described here but using alternative algorithms.

References

Al-Chalabi, M., 1971a, Interpretation of gravity anomalies by nonlinear optimisation: Geophys. Prosp. **20**, 1-16.

_____, 1971b, Some studies relating to nonuniqueness in gravity and magnetic inverse problems: Geophysics **36**, 835-855.

Anderson, W.L., 1977, Electromagnetic fields about a finite electric wire source: U.S. Geol. Surv., Open-File Report, 74-041.

Banerjee, B. and Gupta, S.P.D., 1977, Gravitational attraction of a rectangular parallelepiped: Geophysics **42**, 1053-1055.

Bhattacharyya, B.K., 1978, Computer modelling in gravity and magnetic interpretation: Geophysics **43**, 912.

Cady, J.W., 1980, Calculation of gravity and magnetic anomalies of finite-length right polygonal prisms: Geophysics **45**, 1507-1512.

Chai, Y. and Hinze, W.J., 1988, Gravity inversion of an interface above which the density contrast varies exponentially with depth: Geophysics **53**, 837-845.

Corbato, C.E., 1965, A least-squares procedure for gravity interpretation: Geophysics **30**, 228-233.

Cuer, M. and Bayer, R., 1980, Fortran routines for linear inverse problems: Geophysics **45**, 1706-1719.

Dobrin, M.B., 1960, Introduction to geophysical prospecting: McGraw-Hill Book Co.

Duijndam, A.J.W., 1988, Bayesian estimation in seismic inversion: Geophys. Prosp. **36**, 878-898, 899-918.

Dyrelius, D. and Vogel, A., 1972, Improvement of convergence in iterative gravity interpretation: Geophys. J. Roy. Astr. Soc. **27**, 195-205.

Goodacre, A.K., 1973, Some comments on the calculation of the gravitational and magnetic attraction of a homogeneous rectangular prism: Geophys. Prosp. **21**, 66-69.

Grant, F.S. and West, G.F., 1965, Interpretation theory in applied geophysics: McGraw-Hill Book Co.

Haworth, R.T. and Wells, I., 1980, Interactive computer graphics method for combined interpretation of gravity and magnetic data. Marine Geophys. Res. **4**, 277-290.

Hjelt, S.E., 1973, Experiences with automatic magnetic interpretation using the thick plate model. Geophys. Prosp. **21**, 243-265.

Jackson, D.D., 1979, The use of a priori data to resolve nonuniqueness in linear inversion: Geophys. J. Roy. Astr. Soc. **57**, 137-157.

Johnson, W.W., 1969, A least-squares method of interpreting magnetic anomalies caused by two-dimensional structures: Geophysics **34**, 65-74.

Kellog, O.D., 1929, Foundations of potential theory: Julius Springer. (Reprint 1953, Dover Publications; p. 57 gives a formula for rectangular prism.)

Ku, C.C. and Sharp, J.A., 1983, Werner deconvolution for automated magnetic interpretation and its refinement using Marquardt's inverse modelling: Geophysics **48**, 754-774.

Levenberg, K., 1944, A method for the solution of certain problems in least squares: Quart. Appl. Math. **2**, 164-168.

Marquardt, D.W., 1963, An algorithm for least-squares estimation of nonlinear parameters: J. Soc. Ind. Appl. Math. **11**, 431-441.

McGrath, P.H. and Hood, P.J., 1973, An automatic least-squares multimodel method for magnetic interpretation: Geophysics **38**, 349-358.

Nagy, D. 1966, The gravitational attraction of a right rectangular prism: Geophysics **31**, 362-371, 987.

_____, 1988, A short program for three-dimensional gravity modelling: Acta Geod. Geoph. Mont. Hung. **23**, 449-459.

Nettleton, L.L., 1940, Geophysical prospecting for oil: McGraw-Hill Book Co.

Oldenburg, D. W., 1974, The inversion and interpretation of gravity anomalies: Geophysics **39**, 526-536.

Parker, R.L., 1974, Best bounds on density and depth from gravity data: Geophysics **39**, 644-649.

_____, 1977, Understanding inverse theory: Ann. Rev., Earth Planet. Sci. **5**, 35-64.

Powell, M.J.D., 1964, An efficient method for finding the minimum of a function of several variables without calculating derivatives: Comput. J. **7**, 155-162.

_____, 1965, A method for minimizing a sum of squares of nonlinear functions without calculating derivatives: Comput. J. **7**, 303-307.

Rosenbrock, H.H., 1960, An automatic method for finding the greatest or least value of a function: Comput. J. **3**, 175-184.

Silva, J.B.C. and Hohmann, G.W., 1983, Nonlinear magnetic inversion using a random search method: Geophysics **48**, 1645-1658.

Tabat, T. and Ito, R., 1973, Effective treatment of the interpolation factor in Marquardt's nonlinear least-squares fit algorithm: Computer J. **18**, 250-251.

Talwani, M., 1965, Computation with the help of a digital computer of magnetic anomalies caused by bodies of arbitrary shape: Geophysics **30**, 797.

Telford, W.M., Geldart, L.P., Sherriff, R.E. and Keys, D.A., 1976, Applied geophysics: Cambridge Univ. Press.